

# Phase sensitive information from a planar Josephson junction

Andrew C. Yuan<sup>1</sup> and Steven A. Kivelson<sup>1</sup>

<sup>1</sup>*Department of Physics, Stanford University, Stanford, CA 94305, USA*

(Dated: April 19, 2024)

We analyze both the general symmetry-related and more microscopic considerations that govern the Josephson tunnelling across a finite planar junction between a known  $s$ -wave superconductor and a candidate unconventional superconductor (e.g.,  $d_{x^2-y^2}$ -wave). Due to the finite size of the probe, the Josephson current possesses an edge contribution, which is shown to be the dominant contribution under certain conditions. Thus, the dependence of the edge contribution on the geometry of the junction can serve as a direct probe of the symmetry of the order parameter in the unconventional superconductor.

## I. INTRODUCTION

Famously, phase sensitive measurements [1–4] of the superconducting order in the cuprate high temperature superconductors resolved ongoing debates concerning the symmetry of the order parameter, establishing the key fact that these are  $d$ -wave superconductors. Most of the material systems currently being studied for which similar issues arise are either highly layered (i.e. quasi-two dimensional), like the cuprates, or else are explicitly two dimensional (2D), such as various explicitly two-dimensional layered structures made from van-der Waals materials, especially graphene. The edge junctions of the sort used in the original cuprate experiments are thus often difficult to engineer and sometimes difficult to interpret given the complex nature of such edges. Conversely, many quasi-2D materials cleave relatively easily such that the normal to the surface (henceforth the “ $z$ ” direction) is the least conducting direction. This geometric consideration is still clearer in the case of 2D materials.

### A. Symmetry considerations

With this in mind, we analyze several methods (each easily generalizable) by which  $z$ -direction planar Josephson junctions can be constructed to extract phase sensitive information concerning the symmetry of the order parameter in a candidate unconventional superconductor (SC). (This is somewhat in the spirit of early experiments [5] on the cuprates using twist-junctions, which only now are showing the expected behaviors [6, 7].) Indeed, with somewhat more engineering, the same sort of analysis can be extended to extract information concerning the magnitude of the superconducting gap as a function of position along the Fermi surface (FS).

We consider a planar Josephson junction with the geometry shown in Fig. 1a. The top portion of the junction is a half-plane of what we will assume is a

well-understood simple  $s$ -wave superconductor, and the bottom portion is a full plane of an interesting superconductor, whose order parameter symmetry and gap structure we would like to reveal; as an illustrative example we will assume that it is a  $d_{x^2-y^2}$ -wave SC, but the extension to other symmetries is straightforward. There are two angles that define the geometry of the junction,  $\theta$  which is the relative twist angle between the principle axes of the top and bottom SCs, and  $\phi$  which is the angle of the boundary of the top superconductor relative to the principle axis of the bottom superconductor (see Fig. 3a and 3b). We consider a situation in which the magnitude of the single particle tunnelling between the two superconductors,  $t_{\perp}$ , is weak - i.e. this is assumed to be a planar version of an SIS junction. This means that the energy as a function of  $\alpha$ , the difference in the SC phase across the junction, can be expressed as a series,

$$J(\alpha) = -J_0 - J_1 \cos(\alpha) - J_2 \cos(2\alpha) + \dots \quad (1)$$

where  $J_1 \sim t_{\perp}^2$  plus corrections of order  $t_{\perp}^6$ , while  $J_2 \sim t_{\perp}^4 + \dots$ . Moreover, each  $J_n$  has a bulk contribution, proportional to the area  $A$  of the junction, an edge contribution proportional to the length of the edge,  $L$ , and smaller terms that depend on further details of the shape of the junction. Focusing on the lowest harmonic, we can express  $J_1$  as

$$J_1 = j_{1b}(\theta, \mathbf{g}) \frac{A}{a^2} + j_{1e}(\theta, \phi, \mathbf{g}) \frac{L}{a} + \dots \quad (2)$$

where  $a$  is the lattice constant (which will be set = 1 in the main text),  $j_{1b}/a^2$  is the bulk Josephson coupling per unit area,  $j_{1e}/a$  is the edge contribution per unit length of edge, and  $\dots$  signifies terms that are independent of the size of the junction. Here we have included explicit factors of  $a^n$  so that both  $j_{1b}$  and  $j_{1e}$  have the same units and depend on a set of properties  $\mathbf{g}$  (which will often be left implicit) that characterize the bulk superconducting state of the two superconductors; the bulk  $j_{1b}$  (and higher orders  $j_{2b}, \dots$ ) only depends on the twist angle  $\theta$  since it is

oblivious of the edge, while the edge contribution  $j_{1e}$  depends on both  $\theta, \phi$ .

Whenever the two SCs have different order parameter symmetries, the  $\theta$  and  $\phi$  dependence of  $J_1$  is strong such that it vanishes under some circumstances. For instance, if the  $s$ -wave SC is orthorhombic and the  $d$ -wave SC is tetragonal, then  $j_{1b}$  is generically non-zero [8], but vanishes for any  $\theta$  for which the orthorhombic axis aligns with the gap-nodes of the  $d$ -wave SC. Similar symmetry considerations apply to all odd harmonics,  $J_{2n+1}$ , while the expected angle dependence of  $J_2$  and other even harmonics is much weaker and less revealing. We will primarily explore the symmetry related factors that control  $J_1$ . Moreover, to simplify the discussion, we will take both superconductors to be effectively two-dimensional, i.e. either they are ultra-thin or they have a quasi-2D electronic structure, and that they both have a  $C_4$  rotation symmetry with an axis of rotation perpendicular to the plane.

In this case, since the  $d$ -wave order parameter changes sign and the  $s$ -wave is invariant under a  $C_4$  rotation,  $j_{1b}(\theta) = 0$  for all twist angles  $\theta$ . However,  $C_4$  symmetry is broken by the edge, which implies a non-zero  $j_{1e}$  with a nontrivial  $\theta$  and  $\phi$  dependence. In particular (see Eq. (14) and Appendix (B)),

- 1)  $C_4$  symmetry implies that  $j_{1e} \mapsto -j_{1e}$  under  $\theta \mapsto \theta + \pi/2$  while keeping  $\phi$  fixed.
- 2)  $C_4$  symmetry implies that  $j_{1e} \mapsto -j_{1e}$  under  $\phi \mapsto \phi + \pi/2$  while keeping  $\theta$  fixed.
- 3) Mirror symmetry across the principle diagonal (of either the upper or lower layer) implies that  $j_{1e} \mapsto -j_{1e}$  under  $\theta + \phi \mapsto \pi/2 - (\theta + \phi)$  and  $\phi \mapsto \pi/2 - \phi$

Importantly, the symmetry of an  $s$ - $d$  junction implies that for any fixed  $\theta$ ,  $j_{1e}$  vanishes at a critical edge-angle  $\phi_c(\theta)$  across which  $j_{1e}$  changes sign. (Equally, this can be expressed as a critical twist angle,  $\theta_c(\phi)$ , for given edge angle  $\phi$ .) For example, when the edge is oriented along a symmetry axis, i.e. when  $\phi = 0$  or  $\pi/4 \pmod{\pi/2}$ ,  $j_{1e}$  vanishes whenever  $\theta + \phi = \pi/4 \pmod{\pi/2}$ . Other order parameter symmetries would lead to different patterns of critical angles<sup>1</sup>.

These considerations are illustrated in Fig. 4 which shows results of microscopic calculations described below. Fig. 4b shows the case in which the

FS of the upper SC is relatively small, for which  $j_{1e}(\theta, \phi)$  is approximately a function only of  $\theta + \phi$ , and hence  $\theta + \phi_c(\theta) \approx \pi/4$ <sup>2</sup>. When the FS of the upper layer is larger, the angle dependence of  $j_{1e}(\phi, \theta)$  can be more complicated, and so, correspondingly, is  $\phi_c(\theta)$ , as in the case illustrated in Fig. 4a and 4c.

## B. Microscopic considerations

The explicit calculations for model electronic band-structures, discussed below, reveal a number of more detailed, microscopic features of the two SCs that implicitly affect the Josephson coupling. Particularly important are the magnitude of the two gaps, the structure of the Fermi surfaces and the dependence of the gap function on position along the Fermi surface. Understanding these is essential for making quantitative estimates of the various contributions to  $J_1$ , important for the practical design of such experiments. Conversely, these features can also be exploited to infer more microscopic properties of the SC state.

Of these, the most critical are those that govern the maximum magnitudes of  $j_{1b}$  and  $j_{1e}$ . In cases in which bulk coupling is symmetry allowed, the dependence of  $j_{1b}$  on the SC gap magnitude  $|\Delta|$  is expressible as

$$j_{1b} = \mathcal{J}_{1b} \times \frac{t_{\perp}^2 |\Delta|}{E_F^2} \times \left( \frac{|\Delta|}{E_F} \right)^{\delta} \quad (3)$$

where  $\mathcal{J}_{1b}$  is a dimensionless quantity of order one,  $E_F$  is an appropriate average of the Fermi energies in the two SCs, and the exponent  $\delta = 0$  in the case in which the FSs of the two SCs intersect at discrete points in the Brillouin Zone ( $\mathbb{BZ}$ ), and  $\delta = 1$  when they do not intersect. (Two FSs can be considered *non-intersecting* if the minimum distance between them satisfies the inequality  $\delta k_F a > |\Delta|/E_F$ .) The corresponding expressions for the bulk contribution to  $J_2$  are

$$j_{2b} = \mathcal{J}_{2b} \times \frac{t_{\perp}^4}{|\Delta| E_F^2} \times \left( \frac{|\Delta|}{E_F} \right)^{3\delta} \quad (4)$$

In contrast, because (one component of the) momentum is not conserved for tunnelling at the edge, the magnitude of the edge contribution does not depend as sensitively on the relative positions of the Fermi

<sup>1</sup> For example, if the lower SC were  $g$ -wave instead of  $d$ -wave, then mirror symmetry across the principle axis (of either the upper or lower layer) implies that  $j_{1e} \mapsto -j_{1e}$  under  $\theta + \phi \mapsto \pi - (\theta + \phi)$  and  $\phi \mapsto \pi - \phi$ . Hence,  $j_{1e}$  would vanish at  $\theta + \phi = 0, \pi/4 \pmod{\pi/2}$  at the edge angles  $\phi = 0, \pi/4$  (i.e. at 4 critical angle pairs  $\theta, \phi$ ).

<sup>2</sup> Correspondingly, for an  $s$ - $g$  junction,  $j_{1e}$  would vanish near two critical angles, one with  $\theta + \phi_c \approx 0$  and the other with  $\theta + \phi_c \approx \pi/2$ .

surfaces, so generally

$$j_{1e} = \mathcal{J}_{1e} \times \frac{t_{\perp}^2 |\Delta|}{E_F^2}. \quad (5)$$

Ideally, measurements of the Josephson effect should permit separate evaluation of  $J_1$  and  $J_2$  [9]; in this case, when the bulk contribution to  $J_1$  vanishes by symmetry, the symmetry sensitive angle dependence of  $j_{1e}$  can be used as a phase-sensitive probe of the order parameter of the lower SC. However, even if this is not possible, there exists a range of circumstances in which the edge contribution dominates the total Josephson energy, provided  $t_{\perp}$  is small enough, and if the junction area is not too large. Specifically, so long as  $j_{1b}$  vanishes,

$$\frac{J_1}{J_2} = \frac{\mathcal{J}_{1e}}{\mathcal{J}_{2b}} \left( \frac{|\Delta|}{t_{\perp}} \right)^2 \left( \frac{|\Delta|}{E_F} \right)^{3\delta} \times \frac{La}{A}. \quad (6)$$

In other words, the edge contribution dominates the higher order bulk contribution so long as

$$\frac{A}{La} \ll \left( \frac{|\Delta|}{t_{\perp}} \right)^2 \left( \frac{E_F}{|\Delta|} \right)^{3\delta} \quad (7)$$

Note that this condition is much less stringent if the the FSs do not intersect ( $\delta = 1$ ) than if they do ( $\delta = 0$ ).

### C. Disorder

Since tunneling matrix elements are exponentially sensitive to local details we consider random position dependent variations in the tunnelling matrix element,  $t_{\perp}(\mathbf{r})$ , to be the most important form of disorder. As discussed in greater detail in Appendix (C)), we consider the situation in which there is a mean tunneling matrix,  $t_{\perp} \equiv \overline{t_{\perp}(\mathbf{r})}$ , and a variance,  $\overline{[t_{\perp}(\mathbf{r}) - t_{\perp}][t_{\perp}(\mathbf{r}') - t_{\perp}]}$  that is short-range correlated with mean squared value  $g_{\alpha}^2$  and range  $\xi_{\alpha}$ , where  $\alpha = b, e$  depending on whether we are considering the bulk or edge regions. When computing the disordered-average first order Josephson coupling<sup>3</sup>, it is straightforward to see that the clean-limit and disorder contributions add, i.e.,

$$\bar{J}_1 = (j_{1b} + \delta j_{1b}) \frac{A}{a} + (j_{1e} + \delta j_{1e}) \frac{L}{a} + \dots \quad (8)$$

where  $j_{1b}, j_{1e}$  are given as before.

---

<sup>3</sup> It is not necessary to assume Gaussian distribution since  $\bar{J}_1$  is due to tunneling of a single Cooper pair and thus does not involve higher order correlations

Most importantly, the symmetry considerations that control  $j_{1,\alpha}$  apply to  $\delta j_{1,\alpha}$  as well since, although any given disorder realization locally breaks the point-group symmetries, the ensemble is assumed to have the same symmetries as the crystal, and so therefore do averaged quantities. Even the scaling of the quantities, i.e. when not forbidden by symmetry,  $\delta j_{1\alpha} \sim (g_{\alpha}^2 |\Delta| / E_F^2) (|\Delta| / E_F)^{\delta_{\alpha}}$ , is typically not greatly affected by disorder so long as the correlation length is substantial, i.e.  $k_F \xi \gg 1$ . The essential effect of disorder is to give a momentum boost of order  $\delta k \sim 1/\xi$ . Thus  $\delta_{\alpha}$  is determined in the same way as  $\delta$  where if the distance between the important portions of the Fermi surfaces are spaced by  $\delta k_F > \delta k$ , these portions can be treated as non-intersecting, while otherwise they act as though they are intersecting.

## II. MICROSCOPIC MODEL RESULTS

The geometry of the problem we have in mind, shown in Fig. 1a, consists of a full-plane 2D layer superconductor, on top of which, we place a half-plane superconductor so that there is an edge along  $x = 0$ . We will always compute the Josephson energy perturbatively in powers of the tunnelling Hamiltonian that couples the two layers. However, to make the calculations simpler, we will consider a simplified model consisting of 2 full-plane superconductors, but with a position dependent tunneling Hamiltonian that is nonzero only in the half-plane  $x > 0$  (see Fig. 1b). The latter setup means that the unperturbed Hamiltonian is translationally invariant so that momentum  $\mathbf{k}$  is a good quantum number.

The Hamiltonian thus has the form

$$H = H_0 + H_T \quad (9)$$

where  $H_T$  is the interlayer tunneling Hamiltonian, assumed to be spatially local and to have magnitude  $t_{\perp}$  for  $x > 0$  and vanish for  $x < 0$ . Here  $H_0 = H_0^+ + H_0^-$  describes the decoupled bilayer superconductors with the top/bottom  $H_0^{\pm}$  characterized by the properties  $\mathbf{g}^{\pm} = (\varepsilon^{\pm}, \Delta^{\pm})$  where  $\varepsilon^{\pm}(\mathbf{k})$  are the normal state dispersions and  $\Delta^{\pm}(\mathbf{k})$  are the gap functions. Specifically, in all the numerical calculations we have taken  $E_F = 1$  and

$$\begin{aligned} \varepsilon^+(\mathbf{k}) &= -S_1(\mathbf{k}) - S_2(\mathbf{k}) - \mu^+, \\ \varepsilon^-(\mathbf{k}) &= -S_1(\mathbf{k}) - \mu^-, \\ \Delta^+(\mathbf{k}) &= \Delta_s, \quad \Delta^-(\mathbf{k}) = \Delta_d D(\mathbf{k}), \end{aligned} \quad (10)$$

In terms of the lattice harmonics,  $S_1(\mathbf{k}) = \cos(k_x) + \cos(k_y)$ ,  $S_2(\mathbf{k}) = 2 \cos(k_x) \cos(k_y)$ , and  $D(\mathbf{k}) = \cos(k_x) - \cos(k_y)$ . The values of  $\mu^{\pm}$  used are listed in

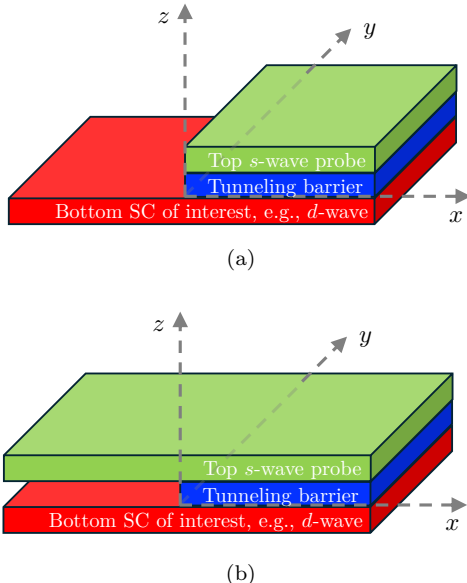


Figure 1. Junction geometry. (a) shows the physical geometry where the upper SC terminates at an edge at  $x = 0$ . (b) shows the model geometry used to simplify microscopic calculations, in which both SCs are infinite, but tunnelling between them is only permitted for  $x > 0$ .

each figure where numerical results are presented; in numerically evaluating the integral expressions for  $j_{1e}$  and  $j_{1b}$  we have typically taken suitably small (compared to the bandwidth) values of  $\Delta_s = 0.12$  and  $\Delta_d = 0.05$ .

The explicit expressions for the various quantities are somewhat involved - they are given explicitly in Sec. (III). The processes that contribute to  $j_{1b}$  to second order in  $t_{\perp}$  involve an intermediate excited state in which one quasi-particle of momentum  $-\mathbf{k}$  is created in one plane, and another with momentum  $\mathbf{k}$  in the other;  $j_{1b}$  is thus obtained by integrating these processes over all  $\mathbf{k}$ . The energy of the excited state is  $E^+(\mathbf{k}) + E^-(\mathbf{k})$  where  $E^{\pm}(\mathbf{k}) = \sqrt{\varepsilon^{\pm}(\mathbf{k})^2 + |\Delta^{\pm}(\mathbf{k})|^2}$ , so the integral tends to be dominated by points in  $\mathbf{k}$  space at which this energy is smallest. For physically reasonable conditions in which  $|\Delta| \ll E_F$ , this means points in  $\mathbf{k}$  space that lie on both Fermi surfaces, if such points exist. The actual integral - including the explicit dependence on the order parameter symmetry - comes through matrix elements related to the usual coherence factors of BCS theory. The calculation of  $j_{2b}$  proceeds similarly, but with intermediate states that involve twice the number of quasi-particles, and correspondingly a double integral over  $\mathbf{k}$  and  $\mathbf{k}'$ .

The structure of the expression for  $j_{1e}$  is similar to that for  $j_{1b}$ , but in this case the edge can act as a source of momentum non-conservation. Consequently, the intermediate states consist of one quasi-

particle with momentum  $-\mathbf{k}$  in one SC and one with momentum  $\mathbf{k} - \mathbf{q}$  in the other, where  $\mathbf{q}$  is a vector perpendicular to the interface. The full result for  $j_{1e}$  thus involves both a two dimensional integral over  $\mathbf{k}$  and a one-dimensional integral over  $\mathbf{q}$ . In this case, the energy of the excited state is  $E^+(\mathbf{k} - \mathbf{q}) + E^-(\mathbf{k})$ , so the integral is dominated by points at which  $\mathbf{k}$  lies on the Fermi surface of one SC and  $\mathbf{k} - \mathbf{q}$  on the Fermi surface of the other.

To confirm these qualitative results we have numerically evaluated the requisite integrals for a simple tight-binding model.

### A. Ideal alignment: $\theta = 0$ and $\phi = 0$

To introduce the problem let us first consider a junction in which the crystalline axes are aligned,  $\theta = 0$ , and the edge is also aligned,  $\phi = 0$ . As discussed following Eqs. (3) and (4), the bulk contributions  $j_{1b}$ ,  $j_{2b}$ , etc. scale differently depending on whether the FS of the top and bottom layers intersect (as shown schematically in Fig. 2a) or not (as in Fig. 2b). In the former case, the integrals of  $\mathbf{k}$  are dominated by regions in the neighborhood of the intersections, where the energy denominators are of order  $|\Delta|$  (and the coherence factors, as well, tend to be relatively large). In the latter case, all energy denominators are of order  $E_F$ , leading to an additional power of  $|\Delta|/E_F$  in the parametric dependence of these quantities, i.e. the exponent  $\delta$  is  $\delta = 0$  in the first case and  $\delta = 1$  in the latter.

In contrast, in computing  $j_{1e}$  one necessarily averages over relative momentum shifts of the Fermi surfaces,  $\mathbf{q}$ , as shown in Figs. 2c and 2d. This typically leads to FS crossings, even when the unshifted FSs are non-overlapping, and is responsible for the fact that the parametric dependences of  $j_{1e}$  are relatively insensitive to details of the FS structure.

### B. General case: $\theta \neq 0$ and $\phi \neq 0$

The analysis of the bulk contribution is relatively simple to extend to non-zero  $\theta$ . In the bulk, even for  $\theta \neq 0$ , the full system (top & bottom) preserves  $C_4$  rotation symmetry (i.e., rotate both layers at the same time) and thus if the two SC order parameters transform differently under rotation,  $j_{1b}(\theta) = 0$  for all  $\theta$ . The scaling of  $j_{2b}(\theta)$  is the same as in Eq. (4) regardless of  $\theta$ . Similarly, for most FS geometries (including both those shown in Figs. 2a and 2b) and for generic values of  $\theta$  and  $\phi$ , the parametric scaling properties of  $j_{1e}(\theta, \phi)$  are as given in Eq. (5). Numerical simulations shown in Fig. 4a and 4b are consistent with this claim.

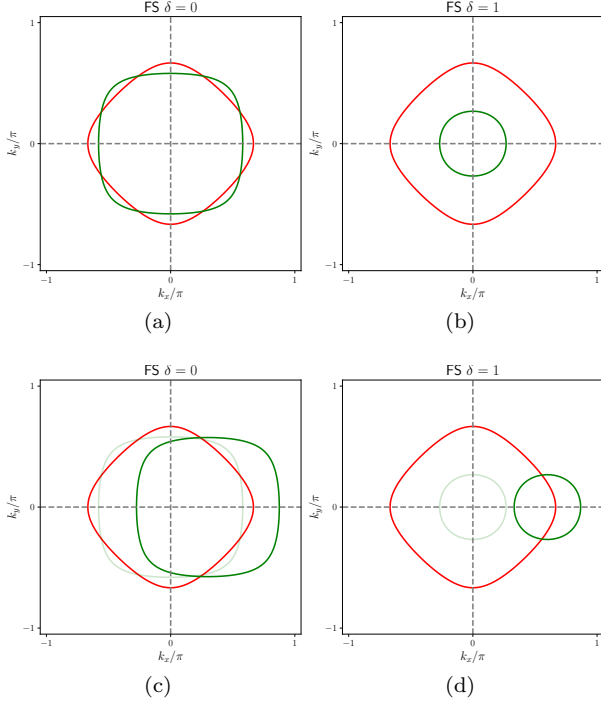


Figure 2. Fermi surface geometries for  $\theta = \phi = 0$ . The red and green contours represent, respectively the top and bottom layer FSs, where (a) illustrates a case in which there are points of intersection and (b) where there are none. In (c) and (d), the top layer FSs from (a) and (b) are shifted by momentum  $\mathbf{q}$  perpendicular to the edge. Here,  $\mu^- = -0.5$  for all subplots, while  $\mu^+ = -0.3$  for (a),(c) and  $\mu^+ = -3$  for (b),(d).

The angle dependence of  $j_{1e}(\theta, \phi)$  can be computed in two morally equivalent methods, which differ from each other due to the lattice geometry (and thus  $\mathbb{BZ}$ ) being non-invariant under general rotation. However, since the calculation will be dominated by momentum near the FS, this difference will be neglected.

- 1) In a coordinate system aligned with the principle axes of the upper SC (as shown in Fig. 3c),  $j_{1e}(\theta, \phi)$  is computed by rotating the bottom layer FS by twist angle  $\theta$  and averaging over momentum boosts  $\mathbf{q}$  of the upper layer in the direction perpendicular to the edge (at angle  $\phi$  with respect to the upper layer).
- 2) Alternatively, in a coordinate system aligned with the lower SC (as shown in Fig. 3d), the  $j_{1e}(\theta, \phi)$  is equivalent to first rotating the upper layer FS by twist angle  $-\theta$  and then averaging over momentum boost  $\mathbf{q}$  perpendicular to the edge (at angle  $\theta + \phi$  with respect to the lower layer).

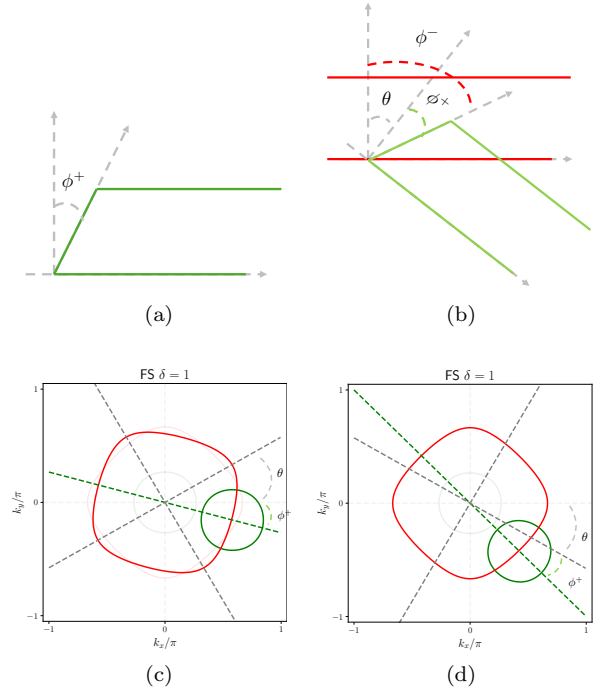


Figure 3. Generic junction geometry: (a).  $\phi$  is the angle of the edge relative to a given principle axis of the upper SC. (b).  $\theta$  is the angle of a principle axis of the lower SC relative to the same principle axis of the upper SC, so the edge is at angle  $\theta + \phi$  relative to the principle axis of the lower SC. (c). In a coordinate system aligned with the principle axes of the upper SC, the heavy green curve indicates the upper layer FS, which is shifted by  $\mathbf{q}$  perpendicular to the edge (i.e. at angle  $\phi$  with respect to the upper layer), while the heavy red curve indicates the bottom layer FS, which is rotated by twist angle  $\theta$ . The pale lines show the original FS as illustrated in Fig. 2b. (d). In a coordinate system aligned with the principle axes of the lower SC, the heavy green curve indicates the upper layer FS, which is first rotated by twist angle  $-\theta$ , then shifted by  $\mathbf{q}$  perpendicular to the edge (i.e. at angle  $\theta + \phi$  with respect to the lower layer). The pale lines show the original FS as illustrated in Fig. 2b.

Since the upper layer is assumed to be a (tetragonal)  $s$ -wave, the latter perspective implies that in the limiting case where the top layer FS is a singular point, the edge effect  $j_{1e}(\theta, \phi)$  only depends on the edge angle  $\theta + \phi$  relative to the lower layer, i.e.,  $j_{1e}(\theta, \phi) = j_{1e}(\theta + \phi)$ . Away from the fine-tuned limit but with the top layer FS sufficiently small, we see that  $j_{1e}(\theta, \phi) \approx j_{1e}(\theta + \phi)$ . Numerical calculations in Fig. 4b confirm that this approximation is valid for small but realistically sized FSs. In particular, Fig. 4d shows that  $j_{1e}$  vanishes near  $\theta + \phi = \pi/4 \bmod \pi/2$  (since  $j_{1e} = 0$  at  $\theta = 0, \phi = \pi/4$  by mirror symmetry across the edge). However, the approximation breaks down for large FSs as shown in Fig.

4a and 4c (Note that the mirror symmetry discussed in the introduction (3)) is still preserved).

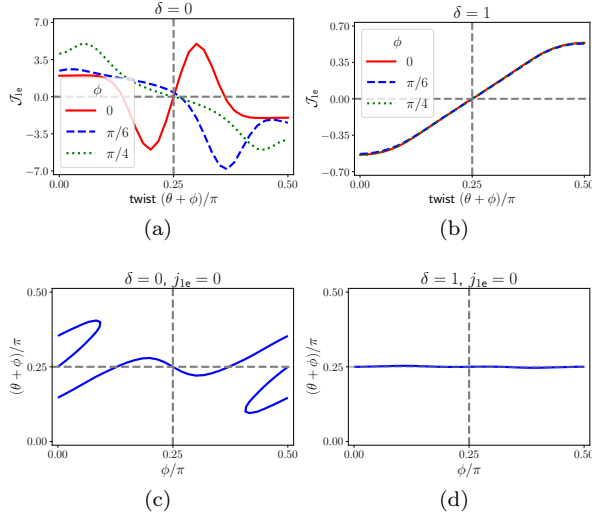


Figure 4. Results computed for the model band structure. For subplots (a),(c), the normal state FSs are assumed to be as in Fig. 2a at ideal alignment  $\theta = \phi = 0$ , while for subplots (b),(d), the normal state FSs are those in Fig. 2b at ideal alignment. (a),(b) plots the dimensionless magnitude of the edge contribution  $\mathcal{J}_{1e}$  as a function of edge angle  $\theta + \phi$  (relative to the lower layer) for distinct edge angles  $\phi = 0, \pi/6, \pi/4$  (relative to upper layer). (c),(d) plots the critical angles at which the edge vanishes  $j_{1e} = 0$  with the  $y$  axis being  $(\theta + \phi)/\pi$ .

### C. Other Considerations

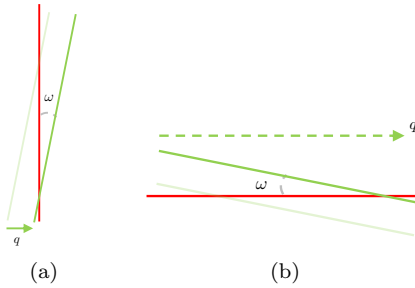


Figure 5. Small angle  $\omega$  intersection of FS.

There are a variety of more detailed features of the electronic structure that effect the magnitude of  $j_{1b}$ ,  $j_{2b}$  and  $j_{1e}$ :

- 1) Number of FS intersections:** As already pointed out, there is a parametric difference between the case of no FS crossings (for which  $\delta = 1$ ) and any finite number (for which  $\delta = 0$ ).

When computing the edge contribution  $j_{1e}$ , the top and bottom FSs can intersect at general momentum shifts  $\mathbf{q}$ . In computing  $j_{1e}$ , if the unshifted ( $\mathbf{q} = 0$ ) FSs are non-intersecting, the shifted FSs will typically intersect at 2 points as shown in Fig. 3c or 3d. Conversely, when the FSs are intersecting  $\delta = 0$ , by  $C_4$  symmetry, the two FSs generally intersect at  $8 = 4 \times 2$  points (2 in each quadrant) and thus there exists a factor  $\times 8$  enhancement in both the bulk and edge contributions (in all orders of perturbation  $j_{1b}, j_{1e}, j_{2b}, \dots$ ).

- 2) Angle of intersection:** The magnitude of the couplings also depends on the angle  $\omega$  between the two intersecting pieces of the FSs. The “nested” case in which  $\omega = 0$ , would lead to a parametrically large (in  $E_F/|\Delta|$ ) enhancement. However, since this is a fine-tuned occurrence, we will consider  $\pi \gg \omega > 0$ , and look at the scaling as  $\omega \rightarrow 0^+$ . It is straightforward to verify that the bulk coefficients are all enhanced by a factor of  $|\pi/\omega|$ . However, the edge coefficient  $j_{1e}$  may or may not gain an extra factor depending on the direction of intersection. For example, in the schematic sketch shown in Fig. 5a,  $j_{1e}$  is not so enhanced, since the factor  $1/\omega$  associated with the particular value of  $\mathbf{k}$  for which the nesting condition is satisfied, is offset by a factor of  $\omega$  from the range of  $\mathbf{q}$  over which this condition is approximately satisfied. Conversely, if the two FS were to intersect horizontally at small angles as sketched in Fig. 5b, then the edge coefficient  $j_{1e}$  gains an extra factor  $1/\omega$  enhancement (not  $1/\omega^2$  since the momentum regime at which the two FS intersect is bounded above, i.e.,  $\Delta q \leq 2\pi$ ).

## III. EXPLICIT INTEGRAL EXPRESSIONS

Here we give some details of the calculations, with particular focus on the calculation of  $j_{1e}$ .

### A. Expression for $j_{1e}$

To second order in perturbation theory with respect to  $t_{\perp}$  (see Appendix (A)),

$$j_{1e} = \underbrace{2t_{\perp}^2 \int_{-\pi}^{\pi} \frac{\delta \mathcal{Z}'(q\hat{\mathbf{x}})}{q^2} \frac{dq}{2\pi}}_{j_{1e}} - \frac{2}{\pi^2} j_{1b} \quad (11)$$

Where  $\hat{\mathbf{x}}$  is the unit vector perpendicular to the edge and

$$\begin{aligned}\delta\mathcal{J}(\mathbf{q}) &= \left[ \frac{|\mathbf{q}|/2}{\sin(|\mathbf{q}|/2)} \right]^2 \frac{j(\mathbf{q}) + j(-\mathbf{q})}{2} - j(\mathbf{0}) \\ j(\mathbf{q}) &= \iint_{\mathbb{B}\mathbb{Z}} f(\mathbf{k}, \mathbf{q}) \frac{d^2\mathbf{k}}{(2\pi)^2} \\ f(\mathbf{k}, \mathbf{q}) &= \frac{1}{E^+(\mathbf{k}-\mathbf{q}) + E^-(\mathbf{k})} \frac{\Delta^+(\mathbf{k}-\mathbf{q})}{E^+(\mathbf{k}-\mathbf{q})} \frac{\Delta^-(\mathbf{k})}{E^-(\mathbf{k})}\end{aligned}\quad (12)$$

Note that  $j_{1b} = t_{\perp}^2 j(\mathbf{q} = \mathbf{0})$  and thus  $j(\mathbf{q})$  would determine  $j_{1b}$  in a case where the two FSs were shifted relative to each other by  $\mathbf{q}$ . We emphasize this relation by writing<sup>4</sup>

$$j(\mathbf{q}) = j[\tau_{\mathbf{q}}\mathbf{g}^+, \mathbf{g}^-] \quad (13)$$

Where  $\tau_{\mathbf{q}}$  denotes the translation operator  $\mathbf{k} \mapsto \mathbf{k} + \mathbf{q}$  in momentum space and  $\mathbf{g}^{\pm} = (\varepsilon^{\pm}, \Delta^{\pm})$  characterize the upper/lower SCs. The  $\theta$  and  $\phi$  dependence of this expression is implicit in the  $\mathbf{k}$  dependence of  $\mathbf{g}^{\pm}$  - in which  $\mathbf{k}$  that appears in Eq. (11) is rotated relative to the geometric  $\hat{\mathbf{x}}, \hat{\mathbf{y}}$  axes. Also note that the edge coefficient  $j_{1e}$  in Eq. (11) includes the bulk coefficient  $j_{1b}$ . However, in most cases,  $j_{1b}$  does not affect the overall scaling (e.g.,  $s, d_{x^2-y^2}$  waves where  $j_{1b} = 0$ ), and thus we will not differentiate the edge coefficient  $j_{1e}$  and the integral term  $\mathcal{J}_{1e}$ .

## B. Scaling

It is known that when the bulk  $j_{1b}$  is symmetry permitted, it scales as Eq. (3). Since the edge contribution  $j_{1e}$  averages over  $j(\mathbf{q})$  for momentum boosts  $\mathbf{q}$  (which determine the bulk  $j_{1b}$  in a case where the two FSs are shifted relative to each other by  $\mathbf{q}$ ), the scaling of  $j_{1e}$  as in Eq. (5) follows from that of the bulk  $j_{1b}$  in Eq. (3). More concretely, assume that the FSs do not intersect ( $\delta = 1$ ) for the moment as shown in Fig. 2b. Then due to the extra suppression factor ( $\delta = 1$ ) in Eq. (3), momentum boosts  $\mathbf{q} \neq \mathbf{0}$  where the relatively shifted FSs intersect will dominate the integral in Eq. (11) as shown in Fig. 6c. Since there is a finite region of  $\mathbf{q} = q\hat{\mathbf{x}}$  where the two FSs intersect at points as shown in Fig. 6a, the edge contribution scales as Eq. (5). Note that the peak  $q_{\text{peak}} \approx 0.4\pi$  in Fig. 6c occurs when the shifted top

layer FS is nearly ‘‘nested’’ with the bottom layer FS as shown in Fig. 6b.

Conversely, if the FS intersect as described by Fig. 2a, the argument is similar, except that the peak occurs at  $q_{\text{peak}} \approx 0$ , since two FSs are already intersecting without any momentum shift.

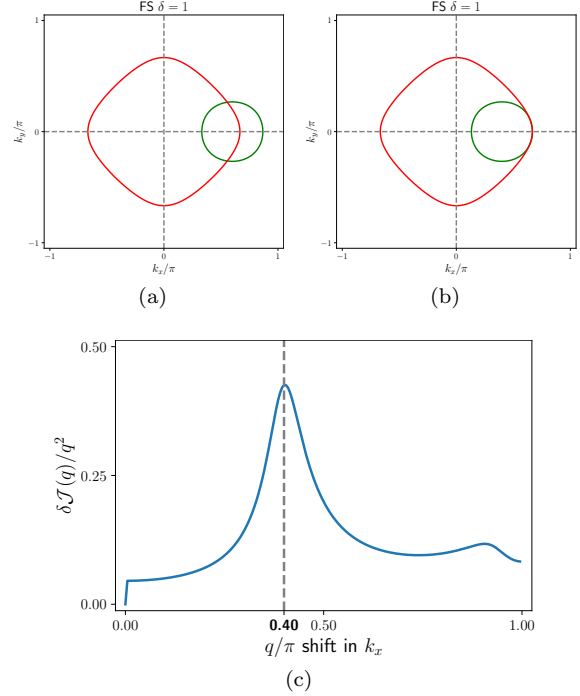


Figure 6. Fermi Surface Shift. The normal state FSs are assumed to be non-intersecting as in Fig. 2b. The green contour in (a) and (b) is the top layer FS shifted by  $\mathbf{q}$  perpendicular to the edge, where (a) shows a generic geometry, corresponding to  $|\mathbf{q}| = 0.6\pi$  and (b) a critical shift  $|\mathbf{q}| \approx 0.4\pi$ . (c) The integrand  $\delta\mathcal{J}(q)/q^2$  appearing in Eq. (11) is shown as a function of momentum shift  $q$ , where  $\delta\mathcal{J}$  is equal to  $\delta\mathcal{J}'$  but in units of the scaling as in Eq. (5).

## C. Rotation and Coordinate Systems

In a coordinate system aligned with the edge along  $x = 0$ , we have

$$j(\mathbf{q}) = j[\tau_{\mathbf{q}}\mathcal{R}_{\phi}\mathbf{g}^+, \mathcal{R}_{\theta+\phi}\mathbf{g}^-] \quad (14)$$

Where  $\mathbf{q}$  is perpendicular to the edge and  $\mathcal{R}_{\phi}$  denotes rotation, i.e.,  $\mathbf{k} \mapsto \mathbf{k}e^{i\phi}$ . The symmetry properties of  $j_{1e}$  claimed in the introduction are then straightforwardly deduced within this representation (see Appendix (B)).

Due to the lattice geometry, the integral over  $\mathbb{B}\mathbb{Z}$  in Eq. (12) is not strictly invariant under arbitrary

<sup>4</sup> Recall, that if a symmetry operator  $S$  (say, translation or rotation) acts on a space (e.g.,  $\mathbf{k} \in \mathbb{B}\mathbb{Z}$ ), then it induces a symmetry operation on functions over the space (e.g.,  $\varepsilon^{\pm}(\mathbf{k})$ ) via the relation  $(S\varepsilon^{\pm})(\mathbf{k}) \equiv \varepsilon^{\pm}(S^{-1}\mathbf{k})$ . Note  $S^{-1}$  is invoked so that the dirac-delta function  $|\mathbf{k}$  centered at momentum  $\mathbf{k}$  is mapped via  $S|\mathbf{k}\rangle = |S\mathbf{k}\rangle$ .

rotation. However, since the integral is dominated by momentum  $\mathbf{k}$  near the FS, we will neglect this difference and thus

$$j(\mathbf{q}) = j[\mathcal{R}_\phi \tau_{\mathcal{R}_{-\phi} \mathbf{q}} \mathbf{g}^+, \mathcal{R}_{\theta+\phi} \mathbf{g}^-] \quad (15)$$

$$= j[\tau_{\mathcal{R}_{-\phi} \mathbf{q}} \mathbf{g}^+, \mathcal{R}_\theta \mathbf{g}^-] \quad (16)$$

Where the 1<sup>st</sup> equality follows from  $\mathcal{R}_{-\phi} \tau_{\mathbf{q}} \mathcal{R}_\phi = \tau_{\mathcal{R}_{-\phi} \mathbf{q}}$ . Note that  $\mathcal{R}_{-\phi} \mathbf{q}$  is along the direction perpendicular to the edge with respect to the upper layer and thus corresponds to a coordinate system aligned with the principle axis of the upper layer (as shown in Fig. 3c). Similarly,

$$j(\mathbf{q}) = j[\mathcal{R}_{-\theta-\phi} \mathcal{R}_\phi \tau_{\mathcal{R}_{-\phi} \mathbf{q}} \mathbf{g}^+, \mathbf{g}^-] \quad (17)$$

$$= j[\tau_{\mathcal{R}_{-(\theta+\phi)} \mathbf{q}} \mathcal{R}_{-\theta} \mathbf{g}^+, \mathbf{g}^-] \quad (18)$$

Where  $\mathcal{R}_{-(\theta+\phi)} \mathbf{q}$  is perpendicular to the edge with respect to the lower layer and thus corresponds to a coordinate system aligned with the principle axis of the lower layer (as shown in Fig. 3d).

#### IV. FINAL REMARKS AND EXPERIMENTAL RECIPE

In a realistic setup, the upper layer  $s$ -wave probe is a finite plane with multiple edges at distinct edge angles rather than a single edge as described by the half-plane in Fig. 1a. In this case, the edge contribution  $j_{1e}$  is the sum of that for each edge of the finite probe and thus an ideal experimental setup would involve a probe geometry forming a long parallelogram so that the edge contribution is mainly due to the pair of long edges (and thus a single edge angle  $\phi$  is well-defined). (Another possibly way<sup>5</sup> to construct such junctions with control over the geometric factors  $\phi$  and  $A/L$  is to use lasers to damage a large planar probe along parallel lines (as sketched in Fig. 7), thereby creating artificially oriented edges within the junction.)

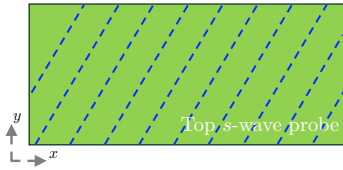


Figure 7. Schematic. The parallel dashed lines resemble the artificially created edges (possibly through laser damage) in the top layer probe (in comparison to Fig. 1).

<sup>5</sup> An idea proposed by Philip Moll in private conversation.

We also note that the ideal  $s$ -wave probe should be one with a single small FS (e.g., SrTiO<sub>3</sub> thin films [10–12]). The reasoning is twofold.

- 1)  $J_1$  will be the dominant contribution in the Josephson current provided that<sup>6</sup> the constraint in Eq. (7) are satisfied. Therefore, if the distance  $\delta k_F$  between the two FS is large, the constraints are much easier to satisfy.
- 2) A smaller FS would increase the resolution<sup>7</sup> of the probe as we vary the twist  $\theta$  and edge angle  $\phi$  described in Fig. 3d and 3c.

There are a large number of circumstances in which unusual SC states are thought to arise in (quasi-) 2D systems, including twisted bilayer graphene [13–16] and its cousins [6, 17–19], for which our proposed approach might prove useful in extracting many important features of the structure of the SC state. One possible application is to determine the order parameter symmetry of Sr<sub>2</sub>RuO<sub>4</sub>, a long-standing enigma spanning over three decades [20]. Indeed, previous proposals have floated the notion of  $d + ig$  pairing symmetry [21–23] where the  $g$ -wave predominantly occupies the  $\alpha, \beta$  bands of Sr<sub>2</sub>RuO<sub>4</sub> [24]. Since the  $\alpha, \beta$  bands comprises  $d_{xz}, d_{yz}$  orbitals, the corresponding  $c$ -axis tunneling parameter  $t_\perp$  is much larger than that of the  $\gamma$  band which consists of  $d_{xy}$  orbitals. Consequently, it is possible that the  $c$ -axis Josephson junction could serve as a means to scrutinize the dominant pairing symmetry on the  $\alpha, \beta$  bands.

Another interesting application is to probe the magnitude of the SC gap along the FS, since the magnitude of the coupling depends rather sensitively on details of the FS structure. For instance, consider the case in which the SC of interest (the lower SC) is trivial ( $s$ -wave) in terms of symmetry, but is thought to have significant angle-dependence of  $\Delta$ . Such examples occur in (slightly) orthorhombic materials where  $s$ -wave is the only irrep of the group symmetry, but since the material is almost tetragonal, it is conceivable that the SC gap inherits a  $d + s$  wave symmetry from the tetragonal group symmetry. We could explore this by choosing the probe (upper) SC to have two Fermi pockets surrounding points  $\pm \mathbf{Q}$  (so that the Fermi pockets intersect the FS of the lower SC); then as a function of  $\theta$ , the portion of the FS of the lower SC that principally dominates  $j_{1b}$

<sup>6</sup> And as usual, if  $j_{1b} = \delta j_{1b} = 0$ , e.g., due to  $C_4$  rotation of an  $s$ - $d$  junction, the edge contributions  $j_{1e}, \delta j_{1e}$  can be used to probe the system via symmetry considerations.

<sup>7</sup> The resolution is maximized in the fine-tuned scenario where the  $s$ -wave probe has a FS consisting of a single point



would change and the angle-dependence of  $\Delta^-(\mathbf{k})$  would be thus revealed. Similarly, by varying  $\phi$ , one can extract similar information from  $j_{1e}$  (though in this case, the Fermi pockets should be away from the FS of the lower SC so that the bulk  $j_{1b}$  contribution is suppressed as in Eq. (3)).

## V. ACKNOWLEDGEMENTS

We acknowledge extremely helpful discussions with Philip Kim, Daryl Schlom, Brad Ramshaw, Kathryn Moler, Phillip Moll, Malcolm Beasley, and Sankar Das Sarma. SAK and AY were supported, in part, by NSF grant No. DMR-2310312 at Stanford.

- 
- [1] W. Neils and D. Van Harlingen, Experimental test for subdominant superconducting phases with complex order parameters in cuprate grain boundary junctions, *Physical review letters* **88**, 047001 (2002).
- [2] C. Tsuei and J. Kirtley, Pairing symmetry in cuprate superconductors, *Reviews of Modern Physics* **72**, 969 (2000).
- [3] C. C. Tsuei, J. R. Kirtley, C. C. Chi, L. S. Yu-Jahnes, A. Gupta, T. Shaw, J. Z. Sun, and M. B. Ketchen, Pairing symmetry and flux quantization in a tricrystal superconducting ring of  $\text{YBa}_2\text{Cu}_3\text{O}_{7-\delta}$ , *Phys. Rev. Lett.* **73**, 593 (1994).
- [4] A. Mathai, Y. Gim, R. C. Black, A. Amar, and F. C. Wellstood, Experimental proof of a time-reversal-invariant order parameter with a  $\pi$  shift in  $\text{YBa}_2\text{Cu}_3\text{O}_{7-\delta}$ , *Phys. Rev. Lett.* **74**, 4523 (1995).
- [5] Q. Li, Y. Tsay, M. Suenaga, R. Klemm, G. Gu, and N. Koshizuka,  $\text{Bi}_2\text{Sr}_2\text{CaCu}_2\text{O}_{8+\delta}$  bicrystal c-axis twist Josephson junctions: a new phase-sensitive test of order parameter symmetry, *Physical review letters* **83**, 4160 (1999).
- [6] S. F. Zhao, X. Cui, P. A. Volkov, H. Yoo, S. Lee, J. A. Gardener, A. J. Akey, R. Engelke, Y. Ronen, R. Zhong, *et al.*, Time-reversal symmetry breaking superconductivity between twisted cuprate superconductors, *Science* **382**, 1422 (2023).
- [7] Y. Zhu, M. Liao, Q. Zhang, H.-Y. Xie, F. Meng, Y. Liu, Z. Bai, S. Ji, J. Zhang, K. Jiang, *et al.*, Presence of *s*-wave pairing in Josephson junctions made of twisted ultrathin  $\text{Bi}_2\text{Sr}_2\text{CaCu}_2\text{O}_{8+x}$  flakes, *Physical Review X* **11**, 031011 (2021).
- [8] R. Kleiner, A. Katz, A. Sun, R. Summer, D. Gajewski, S. Han, S. Woods, E. Dantsker, B. Chen, K. Char, *et al.*, Pair Tunneling from c-Axis  $\text{YBa}_2\text{Cu}_3\text{O}_{7-x}$  to Pb: Evidence for *s*-Wave Component from Microwave Induced Steps, *Physical review letters* **76**, 2161 (1996).
- [9] A. A. Golubov, M. Y. Kupriyanov, and E. Il'Ichev, The current-phase relation in Josephson junctions, *Reviews of modern physics* **76**, 411 (2004).
- [10] E. B. Guedes, S. Muff, M. Fanciulli, A. P. Weber, M. Caputo, Z. Wang, N. C. Plumb, M. Radović, and J. H. Dil, Single spin-polarized Fermi surface in  $\text{SrTiO}_3$  thin films, *Physical Review Research* **2**, 033173 (2020).
- [11] N. Reyren, S. Thiel, A. Cavaglia, L. F. Kourkoutis, G. Hammerl, C. Richter, C. W. Schneider, T. Kopp, A.-S. Ruetschi, D. Jaccard, *et al.*, Superconducting interfaces between insulating oxides, *Science* **317**, 1196 (2007).
- [12] J. A. Bert, B. Kalisky, C. Bell, M. Kim, Y. Hikita, H. Y. Hwang, and K. A. Moler, Direct imaging of the coexistence of ferromagnetism and superconductivity at the  $\text{LaAlO}_3/\text{SrTiO}_3$  interface, *Nature physics* **7**, 767 (2011).
- [13] Y. Cao, V. Fatemi, A. Demir, S. Fang, S. L. Tomarken, J. Y. Luo, J. D. Sanchez-Yamagishi, K. Watanabe, T. Taniguchi, E. Kaxiras, *et al.*, Correlated insulator behaviour at half-filling in magic-angle graphene superlattices, *Nature* **556**, 80 (2018).
- [14] Y. Cao, V. Fatemi, S. Fang, K. Watanabe, T. Taniguchi, E. Kaxiras, and P. Jarillo-Herrero, Unconventional superconductivity in magic-angle graphene superlattices, *Nature* **556**, 43 (2018).
- [15] M. Yankowitz, S. Chen, H. Polshyn, Y. Zhang, K. Watanabe, T. Taniguchi, D. Graf, A. F. Young, and C. R. Dean, Tuning superconductivity in twisted bilayer graphene, *Science* **363**, 1059 (2019).
- [16] E. Y. Andrei and A. H. MacDonald, Graphene bilayers with a twist, *Nature materials* **19**, 1265 (2020).
- [17] A. C. Yuan, Y. Vituri, E. Berg, B. Spivak, and S. A. Kivelson, Inhomogeneity-induced time-reversal symmetry breaking in cuprate twist junctions, *Physical Review B* **108**, L100505 (2023).
- [18] A. C. Yuan, Exactly solvable model of randomly coupled twisted superconducting bilayers, *Physical Review B* **108**, 184515 (2023).
- [19] A. C. Yuan, Absence of floating phase in superconductors with time-reversal symmetry breaking on any lattice, *Physical Review B* **109**, 094509 (2024).
- [20] Y. Maeno, S. Yonezawa, and A. Ramirez, Still mystery after all these years—Unconventional superconductivity of  $\text{Sr}_2\text{RuO}_4$ , *arXiv preprint arXiv:2402.12117* (2024).
- [21] S. A. Kivelson, A. C. Yuan, B. Ramshaw, and R. Thomale, A proposal for reconciling diverse experiments on the superconducting state in  $\text{Sr}_2\text{RuO}_4$ , *npj Quantum Materials* **5**, 43 (2020).
- [22] A. C. Yuan, E. Berg, and S. A. Kivelson, Strain-induced time reversal breaking and half quantum vortices near a putative superconducting tetracritical point in  $\text{Sr}_2\text{RuO}_4$ , *Physical Review B* **104**, 054518 (2021).
- [23] R. Willa, M. Hecker, R. M. Fernandes, and J. Schmalian, Inhomogeneous time-reversal symmetry breaking in  $\text{Sr}_2\text{RuO}_4$ , *Physical Review B* **104**, 024511 (2021).
- [24] A. C. Yuan, E. Berg, and S. A. Kivelson, Multiband mean-field theory of the *d+ig* superconductivity scenario in  $\text{Sr}_2\text{RuO}_4$ , *Physical Review B* **108**, 014502

(2023).

**Appendix A: Computing  $j_{1e}$** 

Using the simplified setup shown in Fig. 1b, we take each layer to have linear size  $L = 2\ell$  (with even  $\ell$  for simplicity) and adopt periodic boundary conditions so that translation symmetry is preserved. The general formula for the first order Josephson coupling  $J_1$  is then given by

$$J_1 = \sum_{\mathbf{k}', \mathbf{k} \in \mathbb{B}\mathbb{Z}} |T(\mathbf{k}', \mathbf{k})|^2 f(\mathbf{k}, \mathbf{k} - \mathbf{k}') \quad (\text{A1})$$

where  $f(\mathbf{k}, \mathbf{q})$  is given in Eq. (12) and  $T(\mathbf{k}', \mathbf{k})$  is the interlayer tunneling matrix in momentum space, i.e., the tunneling matrix is diagonal in real space  $\mathbf{r}$  and  $= t_\perp$  only on the half-plane  $x \geq 0$ , and thus

$$\frac{T(\mathbf{k}', \mathbf{k})}{t_\perp} = \frac{1}{L^2} \sum_{x \geq 0} e^{-i(\mathbf{k}' - \mathbf{k})\mathbf{r}} \quad (\text{A2})$$

$$\begin{aligned} &= \frac{1}{L} 1\{\mathbf{k} - \mathbf{k}' = q\hat{\mathbf{x}}\} \sum_{x=0}^{\ell-1} e^{iqx} \\ &= \frac{1}{2} 1\{\mathbf{k}' = \mathbf{k}\} + 1\{\mathbf{k} - \mathbf{k}' = q\hat{\mathbf{x}}, q \text{ odd}\} \frac{2}{L} \frac{1}{1 - e^{iq}} \end{aligned} \quad (\text{A3})$$

where the momentum transfer during tunnelling  $\{q \text{ odd}\}$  is short for  $q = 2\pi m/L$  where  $m$  is an odd integer in  $\{-\ell, \dots, \ell - 1\}$ . Therefore,

$$J_1 = \underbrace{\frac{t_\perp^2}{4} \sum_{\mathbf{k} \in \mathbb{B}\mathbb{Z}} f(\mathbf{k}, \mathbf{q} = \mathbf{0})}_{(1)} + t_\perp^2 \underbrace{\sum_{q \text{ odd}, \mathbf{k} \in \mathbb{B}\mathbb{Z}} \frac{1}{L^2} \frac{1}{\sin^2(q/2)} f(\mathbf{k}, q\hat{\mathbf{x}})}_{(2)}. \quad (\text{A4})$$

Note that

$$\frac{1}{L^2} \sum_{\mathbf{k} \in \mathbb{B}\mathbb{Z}} f(\mathbf{k}, q\hat{\mathbf{x}}) = \underbrace{\iint_{\mathbb{B}\mathbb{Z}} f(\mathbf{k}, q\hat{\mathbf{x}})}_{j(q\hat{\mathbf{x}})} + O\left(\frac{1}{L^2}\right). \quad (\text{A5})$$

Where we have kept the error term since we are interested in not only the leading order term  $\sim L^2$  but also the next to leading term,  $\sim L$ . Hence, the first term in Eq. (A4) contributes a bulk effect, i.e.,

$$(1) = \frac{t_\perp^2}{4} j(\mathbf{0}) L^2 + O(1). \quad (\text{A6})$$

The second term is given by

$$(2) = t_\perp^2 \sum_{q \text{ odd}} \frac{1}{\sin^2(q/2)} \left[ j(q\hat{\mathbf{x}}) + O\left(\frac{1}{L^2}\right) \right]. \quad (\text{A7})$$

It turns out that this also contains a ( $L^2$ ) bulk contribution in addition to an edge ( $L^1$ ) contribution. To see this, focus on the small  $q$  portion of the sum, and observe that

$$\sum_{q \text{ odd}} \frac{1}{q^2} = \frac{L^2}{2\pi^2} \underbrace{\sum_{m=0}^{\ell/2-1} \frac{1}{(2m+1)^2}}_{\leq \pi^2/8}. \quad (\text{A8})$$

Since the summation is bounded by  $\pi^2/8$  in the  $L \rightarrow \infty$  limit, we see that the  $1/q^2$  divergence is at most  $O(L^2)$  and thus we can drop the error term since it is now  $O(1)$ , i.e.,

$$(2) = t_{\perp}^2 \sum_{q \text{ odd}} \frac{j(q\hat{\mathbf{x}})}{\sin^2(q/2)} + O(1) \quad (\text{A9})$$

To treat the first term in Eq. (A9), write

$$\mathcal{J}(\mathbf{q}) = \left( \frac{|\mathbf{q}|/2}{\sin(|\mathbf{q}|/2)} \right)^2 j(\mathbf{q}) \quad (\text{A10})$$

$$\delta \mathcal{J}(\mathbf{q}) = \frac{1}{2} (\mathcal{J}(\mathbf{q}) + \mathcal{J}(-\mathbf{q}) - \mathcal{J}(\mathbf{0})) \quad (\text{A11})$$

Where we note that  $\mathcal{J}(\mathbf{0}) = j(\mathbf{0})$ . Therefore,

$$\sum_{q \text{ odd}} \frac{j(q\hat{\mathbf{x}})}{\sin^2(q/2)} = j(\mathbf{0}) \sum_{q \text{ odd}} \frac{4}{q^2} + \sum_{q \text{ odd}} \frac{4}{q^2} \delta \mathcal{J}(q\hat{\mathbf{x}}) \quad (\text{A12})$$

Note that the 2<sup>nd</sup> term is now well-regulated in the thermodynamic limit  $L \rightarrow \infty$  since  $\delta \mathcal{J}(q\hat{\mathbf{x}}) \propto q^2$  for small  $q$ , and thus

$$\frac{1}{L} \sum_{q \text{ odd}} \frac{4}{q^2} \delta \mathcal{J}(q\hat{\mathbf{x}}) = 2 \int_{-\pi}^{\pi} \frac{\delta \mathcal{J}(q\hat{\mathbf{x}})}{q^2} \frac{dq}{2\pi} + O\left(\frac{1}{L}\right). \quad (\text{A13})$$

The first term in Eq. (A12) is  $O(L^2)$  and thus makes another (equal) contribution to the bulk effect as expected. To obtain the edge effect, we must consider higher orders of  $1/L$  in the summation

$$\sum_{m=0}^{\ell/2-1} \frac{1}{(2m+1)^2} = \left[ \sum_{m=0}^{\infty} - \sum_{m \geq \ell/2} \right] \frac{1}{(2m+1)^2} \quad (\text{A14})$$

$$= \frac{\pi^2}{8} - \sum_{m \geq \ell/2} \frac{1}{(2m+1)^2} \quad (\text{A15})$$

Note that the 2<sup>nd</sup> term scales like

$$\int_{s>\ell} \frac{ds}{s^2} \sim \frac{1}{L} \quad (\text{A16})$$

Therefore, to obtain the edge effect, we write

$$\sum_{m \geq \ell/2} \frac{1}{(2m+1)^2} = \sum_{m \geq \ell/2} \frac{1}{(2m+1)(2m-1)} + O\left(\frac{1}{L^2}\right) \quad (\text{A17})$$

Where the difference is  $O(1/L^2)$  since it scales like

$$\int_{s>\ell} \frac{ds}{s^3} \sim \frac{1}{L^2} \quad (\text{A18})$$

It is then straightforward to verify that

$$\sum_{m \geq \ell/2} \frac{1}{(2m+1)(2m-1)} = \frac{1}{2} \sum_{m \geq \ell/2} \left( \frac{1}{2m-1} - \frac{1}{2m+1} \right) \quad (\text{A19})$$

$$= \frac{1}{2} \frac{1}{\ell-1} \quad (\text{A20})$$

Putting everything together, we find that in the limit  $L \rightarrow \infty$ ,

$$\sum_{q \text{ odd}} \frac{4}{q^2} = \frac{1}{4}L^2 - \frac{2}{\pi^2}L + O(1) \quad (\text{A21})$$

Hence,

$$(2) = \frac{t_{\perp}^2}{4} j(\mathbf{0}) \times L^2 \quad (\text{A22})$$

$$+ t_{\perp}^2 \left[ 2 \int_{-\pi}^{\pi} \frac{\delta \mathcal{J}(q\hat{\mathbf{x}})}{q^2} \frac{dq}{2\pi} - \frac{2}{\pi^2} j(\mathbf{0}) \right] \times L \quad (\text{A23})$$

$$+ O(1). \quad (\text{A24})$$

This is of the form as the expressions given in the text,

$$J_1 = j_{1b}A + j_{1e}L + O(1) \quad (\text{A25})$$

with  $A = L^2/2$  the area of half-plane.

## Appendix B: Symmetries

In the introduction, we claimed that

- 1)  $C_4$  symmetry of the lower  $d$  wave implies that  $j_{1e} \mapsto -j_{1e}$  under  $\theta \mapsto \theta + \pi/2$  while keeping  $\phi$  fixed.
- 2)  $C_4$  symmetry of the  $s, d$  wave junction implies that  $j_{1e} \mapsto -j_{1e}$  under  $\phi \mapsto \phi + \pi/2$  while keeping  $\theta$  fixed
- 3) Mirror symmetry across the principle diagonal (of either the upper or lower layer) implies that  $j_{1e} \mapsto -j_{1e}$  under  $\theta + \phi \mapsto \pi/2 - (\theta + \phi)$  and  $\phi \mapsto \pi/2 - \phi$

Here we provide a short proof using the coordinate system with the edge aligned along  $x = 0$ . Claims (1) and (2) follow trivially from the representation in Eq. (14) and thus we will focus on claim (3). Let  $\mathcal{D}$  denote the mirror symmetry across the principle diagonal, i.e.,  $\mathbf{k} \equiv |\mathbf{k}|e^{i\alpha} \mapsto |\mathbf{k}|e^{i(\pi/2-\alpha)}$ . Since the upper SC is an  $s$ -wave and the lower is a  $d$  wave, we find that

$$-j[\tau_{q\hat{\mathbf{x}}}\mathcal{R}_{\phi}\mathbf{g}^+, \mathcal{R}_{\theta+\phi}\mathbf{g}^-] = j[\tau_{q\hat{\mathbf{x}}}\mathcal{R}_{\phi}\mathcal{D}\mathbf{g}^+, \mathcal{R}_{\theta+\phi}\mathcal{D}\mathbf{g}^-] \quad (\text{B1})$$

$$= j[\tau_{q\hat{\mathbf{x}}}\mathcal{D}\mathcal{R}_{-\phi}\mathbf{g}^+, \mathcal{D}\mathcal{R}_{-(\theta+\phi)}\mathbf{g}^-] \quad (\text{B2})$$

$$= j[\tau_{q\hat{\mathbf{y}}}\mathcal{R}_{-\phi}\mathbf{g}^+, \mathcal{R}_{-(\theta+\phi)}\mathbf{g}^-] \quad (\text{B3})$$

$$= j[\mathcal{R}_{-\pi/2}\tau_{-q\hat{\mathbf{x}}}\mathcal{R}_{\pi/2}\mathcal{R}_{-\phi}\mathbf{g}^+, \mathcal{R}_{-(\theta+\phi)}\mathbf{g}^-] \quad (\text{B4})$$

$$= j[\tau_{-q\hat{\mathbf{x}}}\mathcal{R}_{\pi/2-\phi}\mathbf{g}^+, \mathcal{R}_{\pi/2-(\theta+\phi)}\mathbf{g}^-] \quad (\text{B5})$$

The claim then follows from Eq. (11) and (12).

## Appendix C: Disorder

In each order of perturbation theory, what enters are the tunneling matrix elements  $T(\mathbf{k}, \mathbf{k}')$  for transferring an electron from a Bloch state with crystal momentum  $\mathbf{k}$  in the upper layer to  $\mathbf{k}'$  in the lower layer - and naturally  $T^*(\mathbf{k}, \mathbf{k}')$  associated with the time-reversed process. (In more general circumstances, there could be multiple band indices associated with the single particle states of the decoupled layers, which we ignore here for simplicity.)

When we consider the problem with disorder, we assume that mesoscopic effects can be neglected, or in other words we compute the configuration average of the various contributions to the Josephson coupling,  $\bar{J}_n$ . For the leading order term,  $\bar{J}_1$ , this means the results depend on  $\overline{T(\mathbf{k}', \mathbf{k})T(-\mathbf{k}', -\mathbf{k})}$ , while higher

order terms  $n \geq 2$  need knowledge of higher order moments of  $T$ . We will further always assume that the tunnelling Hamiltonian is time-reversal invariant, in which case  $\overline{T(\mathbf{k}', \mathbf{k})T(-\mathbf{k}', -\mathbf{k})} = \overline{|T(\mathbf{k}', \mathbf{k})|^2}$ . In particular, for finite  $L$  so that  $\mathbf{k}$  is a discrete variable,

$$\bar{J}_1 = \sum_{\mathbf{k}', \mathbf{k} \in \mathbb{B}\mathbb{Z}} \overline{|T(\mathbf{k}', \mathbf{k})|^2} f(\mathbf{k}, \mathbf{k} - \mathbf{k}') \quad (\text{C1})$$

where  $f(\mathbf{k}, \mathbf{q})$ , which depends only on the properties of the decoupled layers, is given in Eq. (12).

For the purposes of explicit calculations, as in the clean limit, we will assume that the tunnelling is defined by a local matrix element,  $t(\mathbf{r})$ , so that

$$T(\mathbf{k}, \mathbf{k}') \equiv \frac{1}{L^2} \sum_{\mathbf{r}} t(\mathbf{r}) e^{-i(\mathbf{k} - \mathbf{k}')\mathbf{r}}. \quad (\text{C2})$$

To account for disorder in the tunnelling matrix elements, we assume a random distribution with mean  $\overline{t(\mathbf{r})}$  and variance:

$$\overline{t(\mathbf{r})t(\mathbf{r}') - \overline{t(\mathbf{r})} \times \overline{t(\mathbf{r}')} = \sigma(\mathbf{r}, \mathbf{r}'), \quad (\text{C3})$$

In computing the first order Josephson coupling, the precise form of the distribution of  $t(\mathbf{r})$ 's is unimportant - only these moments matter.

- 1) As a reminder, a system without edges only possesses a bulk contribution and thus it is standard to take the mean  $\overline{t(\mathbf{r})} = t_{\perp}$  and variance  $\sigma(\mathbf{r}, \mathbf{r}') = \sigma_b(\mathbf{r} - \mathbf{r}')$  so that

$$\overline{|T(\mathbf{k}', \mathbf{k})|^2} = |t_{\perp}|^2 \delta_{\mathbf{k}, \mathbf{k}'} + \frac{1}{L^2} \Sigma_b(\mathbf{k} - \mathbf{k}') \quad (\text{C4})$$

where the first term denotes the clean-limit contribution proportional to  $|t_{\perp}|^2$ , and  $\Sigma_b$ , which is the Fourier transform of  $\sigma_b$ , reflects the point-to-point variations in the tunnelling matrix elements, and so is characterized by a magnitude,  $\Sigma_b(\mathbf{0})$ , and a width in  $\mathbf{k}$ -space  $|\delta\mathbf{k}| \sim 1/\xi$ .

- 2) In comparison, when an edge is present (as shown in Fig. 1b), we need to take into account the lack of (even average) translational symmetry and thus take

$$\overline{t(\mathbf{r})} = t_{\perp} \Theta(x), \quad \sigma(\mathbf{r}, \mathbf{r}') = \sigma_e(\mathbf{r} - \mathbf{r}') \Theta(X) \quad (\text{C5})$$

where  $\Theta$  is the Heaviside function and  $X = (x + x')/2$  is the average displacement from the edge<sup>8</sup>. In particular, if  $\mathbf{r}$  and  $\mathbf{r}'$  are far from the edge, the disorder correlation reduces to a bulk term  $\sigma(\mathbf{r}, \mathbf{r}') = \sigma_e(\mathbf{r} - \mathbf{r}')$  (For example, it is reasonable to imagine  $\sigma(\mathbf{r}, \mathbf{r}') = \sigma_b(\mathbf{r} - \mathbf{r}') \Theta(X)$ ).<sup>9</sup>

In either case, the expression for  $\overline{|T(\mathbf{k}', \mathbf{k})|^2}$ , and hence for  $\bar{J}_1$  is expressible as the sum of a term proportional to  $|t_{\perp}|^2$  and the second term which is proportional to  $\sigma$  (or its Fourier transform  $\Sigma$ ) which reflects the presence of disorder:

$$\bar{J}_1 = (j_{1b} + \delta j_{1b}) \times A + (j_{1e} + \delta j_{1e}) \times L + O(1) \quad (\text{C6})$$

Where  $j_{1b}, j_{1e}$  are the values from the clean limit and  $\delta j_{1b}, \delta j_{1e}$  originate from the disorder correlation.

<sup>8</sup> There is a subtlety in defining  $\Theta(X)$  since  $X \mapsto X + L/2$  under periodic translation  $x \mapsto x + L$ . This subtlety introduces an innate UV cutoff which results in an edge term contribution from the disorder. We discuss this in more detail in Appendix (C2).

<sup>9</sup> Although the current form of disorder  $\sigma(\mathbf{r}, \mathbf{r}')$  gives both a bulk  $\delta j_{1b}$  and edge  $\delta j_{1e}$  contribution, it is not technically correct since only  $\sigma_e$  provides a correlation length

and disorder strength, while in principle, the characterizations could be distinct for the edge and bulk. A more accurate form would be  $\sigma(\mathbf{r}, \mathbf{r}') = \sigma_e(\mathbf{r} - \mathbf{r}') \mathbb{1}\{0 \leq X < \text{UV cutoff}\} + \sigma_b(\mathbf{r} - \mathbf{r}') \Theta(X)$  where the UV cutoff is on the length scale of the lattice constant  $a$  (characterizes the width of the edge), so that the first term provides the dominant edge contribution  $\delta j_{1e}$  and the second provides the bulk contribution  $\delta j_{1b}$ .

### 1. Review: Bulk with Disorder

When considering the bulk disorder, we have

$$\Sigma_b(\mathbf{q}) = \frac{1}{L^2} \sum_{\mathbf{r}} \sigma_b(\mathbf{r}) e^{-i\mathbf{q}\mathbf{r}} \quad (\text{C7})$$

and thus

$$\delta j_{1b} \times A + O(1) = \frac{1}{L^2} \sum_{\mathbf{k}', \mathbf{k} \in \mathbb{B}\mathbb{Z}} \Sigma_b(\mathbf{k} - \mathbf{k}') f(\mathbf{k}, \mathbf{k} - \mathbf{k}') \quad (\text{C8})$$

$$= \sum_{\mathbf{q} \in \mathbb{B}\mathbb{Z}} \Sigma_b(\mathbf{q}) j(\mathbf{q}) + O(1) \quad (\text{C9})$$

$$= A \times \iint_{\mathbf{q} \in \mathbb{B}\mathbb{Z}} \Sigma_b(\mathbf{q}) j(\mathbf{q}) \frac{d^2 \mathbf{q}}{(2\pi)^2} + O(1) \quad (\text{C10})$$

$$\delta j_{1b} = \iint_{\mathbf{q} \in \mathbb{B}\mathbb{Z}} \Sigma_b(\mathbf{q}) j(\mathbf{q}) \frac{d^2 \mathbf{q}}{(2\pi)^2} \quad (\text{C11})$$

Where the second equality uses Eq. (A5) and that  $\sigma_b(\mathbf{r}) = O(1)$  (i.e.,  $\Sigma_b(\mathbf{q}) = O(1)$ ).

If  $\sigma_b(\mathbf{r})$  has a characteristic correlation length  $\xi_b$  (e.g.,  $\sigma_b(\mathbf{r})$  is of Gaussian form), then its Fourier transform has correlation length  $1/\xi_b$ . If  $1/\xi_b$  is smaller than the distance  $\delta k_F$  between the FSs so that even after momentum boost, the two FS do not intersect for  $|\mathbf{q}| < 1/\xi_b$ . Therefore, when so long as the result does not vanish by symmetry (i.e. under the same constraints that apply in the clean limit), the disorder contribution scales like

$$\delta j_{1b} \sim \frac{g_b^2 |\Delta|}{E_F^2} \times \left( \frac{|\Delta|}{E_F} \right), \quad (\text{C12})$$

where  $g_b^2 \sim \Sigma_b(\mathbf{r}) \sim \Sigma_b(\mathbf{q})$  is the characteristic disorder strength (replaces the tunneling parameter  $t_{\perp}$  in Eq. (3)). In all other scenarios, the extra suppression factor vanishes so that

$$\delta j_{1b} \sim \frac{g_b^2 |\Delta|}{E_F^2} \times \left( \frac{|\Delta|}{E_F} \right)^{\delta_b} \quad (\text{C13})$$

Where  $\delta_b = 1$  if the FS are non-intersecting ( $\delta = 1$ , i.e.,  $\delta k_F \gtrsim |\Delta|/E_F$ ) and  $\delta k_F \gtrsim 1/\xi_b$ .

### 2. Edge with Disorder

When consider an edge, it is natural to model the disorder<sup>10</sup> via

$$\sigma(\mathbf{r}, \mathbf{r}') = \sigma_e(\mathbf{r} - \mathbf{r}') \Theta(X), \quad X = \frac{x + x'}{2} \quad (\text{C14})$$

Note that the variance  $\sigma(\mathbf{r}, \mathbf{r}')$  should be  $L$ -periodic with respect to  $\mathbf{r}, \mathbf{r}'$ . However, as currently defined, the average position  $X \mapsto X + L/2$  under translation  $x \mapsto x + L$  and  $x' \mapsto x'$ , and thus we need to define the variance more carefully. The simplest way is to define  $[x]$  as the  $L$ -modulo of the  $x$  position so that  $[x] \in \mathbb{Z}$

<sup>10</sup> Although the current form of disorder  $\sigma(\mathbf{r}, \mathbf{r}')$  gives both a bulk  $\delta j_{1b}$  and edge  $\delta j_{1e}$  contribution, it is not technically correct since only  $\sigma_e$  provides a correlation length and disorder strength, while in principle, the characterizations could be distinct for the edge and bulk. A more accurate form would be  $\sigma(\mathbf{r}, \mathbf{r}') = \sigma_e(\mathbf{r} - \mathbf{r}') 1\{0 \leq X <$

$UV \text{ cutoff}\} + \sigma_b(\mathbf{r} - \mathbf{r}') \Theta(X)$  where the UV cutoff is on the length scale of the lattice constant  $a$  (characterizes the width of the edge), so that the first term provides the dominant edge contribution  $\delta j_{1e}$  and the second provides the bulk contribution  $\delta j_{1b}$ .

and within the interval  $-\ell \leq [x] < \ell$  (where continuing the notation in Appendix (A) and taking  $L = 2\ell$ ), and replace  $\Theta(X)$  with

$$\Theta\left(\frac{[x] + [x']}{2}\right) \equiv 1 \left\{ 0 \leq \left(\frac{[x] + [x']}{2}\right) \in \mathbb{R}\right\} < \ell \right\} \quad (\text{C15})$$

With this modification, one can compute the Fourier transform, i.e.,

$$\Sigma(\mathbf{q}) = \frac{1}{L^4} \sum_{\mathbf{r}, \mathbf{r}'} \sigma_e(\mathbf{r} - \mathbf{r}') e^{-i\mathbf{q}(\mathbf{r}' - \mathbf{r})} \Theta\left(\frac{[x'] + [x]}{2}\right) \quad (\text{C16})$$

Where the summation  $\mathbf{r}, \mathbf{r}'$  is over  $\{-\ell, \dots, \ell - 1\}^2$ , respectively. Since the integrand is  $L$ -periodic with respect to  $\mathbf{r}, \mathbf{r}'$ , we have

$$\Sigma(\mathbf{q}) = \frac{1}{L^3} \sum_{\delta\mathbf{r} \equiv (\delta x, \delta y) \in \{-\ell, \dots, \ell - 1\}^2} \sigma_e(\delta\mathbf{r}) e^{-i\mathbf{q}\delta\mathbf{r}} \sum_{-\ell \leq (x \in \mathbb{Z}) < \ell} \Theta\left(\frac{[x + \delta x] + [x]}{2}\right) \quad (\text{C17})$$

$$= \frac{1}{L^3} \sum_{\delta\mathbf{r}} \sigma_e(\delta\mathbf{r}) e^{-i\mathbf{q}\delta\mathbf{r}} (\ell - 1\{\delta x \text{ odd}\}) \quad (\text{C18})$$

$$= \frac{1}{2} \Sigma_e(\mathbf{q}) - \frac{1}{2L} \underbrace{\left[ \frac{2}{L^2} \sum_{\delta\mathbf{r}} \sigma_e(\delta\mathbf{r}) 1\{\delta x \text{ odd}\} e^{-i\mathbf{q}\delta\mathbf{r}} \right]}_{= \Sigma_e(\mathbf{q}) + O(1/L^2)} \quad (\text{C19})$$

where  $\{\delta x \text{ odd}\}$  is short for summing only over odd integers  $\delta x$  within the interval  $\delta x \in \{-\ell, \dots, \ell - 1\}$ . Note the first term will provide the bulk disorder  $\delta j_{1b}$  (compare with Eq. (C7)), while the second term will contribute to the edge disorder  $\delta j_{1e}$ . More specifically,

$$\delta j_{1b} \times A + \delta j_{1e} \times L + O(1) = \frac{1}{L^2} \sum_{\mathbf{k}', \mathbf{k} \in \mathbb{B}\mathbb{Z}} \Sigma(\mathbf{k} - \mathbf{k}') f(\mathbf{k}, \mathbf{k} - \mathbf{k}') \quad (\text{C20})$$

$$= \sum_{\mathbf{q} \in \mathbb{B}\mathbb{Z}} \Sigma(\mathbf{q}) j(\mathbf{q}) + O(1) \quad (\text{C21})$$

$$= A \times \iint_{\mathbf{q} \in \mathbb{B}\mathbb{Z}} \Sigma_e(\mathbf{q}) j(\mathbf{q}) \frac{d^2\mathbf{q}}{(2\pi)^2} + L \times \frac{1}{2} \iint_{\mathbf{q} \in \mathbb{B}\mathbb{Z}} \Sigma_e(\mathbf{q}) j(\mathbf{q}) \frac{d^2\mathbf{q}}{(2\pi)^2} + O(1) \quad (\text{C22})$$

Where we used the fact that the “effective area” of a half-plane is  $A = L^2/2$ . Hence,

$$\delta j_{1b} = 2\delta j_{1e} = \iint_{\mathbf{q} \in \mathbb{B}\mathbb{Z}} \Sigma_e(\mathbf{q}) j(\mathbf{q}) \frac{d^2\mathbf{q}}{(2\pi)^2} \quad (\text{C23})$$

Using a similar argument for the bulk disorder, we find that

$$\delta j_{1b}, \delta j_{1e} \sim \frac{g_e^2 |\Delta|}{E_F^2} \times \left(\frac{|\Delta|}{E_F}\right)^{1\{\delta k_F \gtrsim 1/\xi_e, |\Delta|/E_F\}} \quad (\text{C24})$$